Title

Intensified Positive Arctic—Methane Feedback under IPCC Climate Scenarios in the 21st Century

Authors

Wang, Yihui

He, Liyuan

Liu, Jianzhao

et al.

Publication Date

2024

DOI

10.34133/ehs.0185

Peer reviewed

Ecosystem Health and Sustainability
A SCIENCE PARTNER JOURNAL

REVIEW ARTICLE

Intensified Positive Arctic–Methane Feedback under IPCC Climate Scenarios in the 21st Century

Yihui Wang[1], Liyuan He[1], Jianzhao Liu[2], Kyle A. Arndt[3], Jorge L. Mazza Rodrigues[4], Donatella Zona[1], David A. Lipson[1], Walter C. Oechel[1], Daniel M. Ricciuto[5], Stan D. Wullschleger[5], and Xiaofeng Xu[1*]

[1]Department of Biology, San Diego State University, San Diego, CA 92182, USA. [2]Key Laboratory of Wetland Ecology and Environment, Northeast Institute of Geography and Agroecology, Chinese Academy of Sciences, Changchun, Jilin 130021, China. [3]Woodwell Climate Research Center, Falmouth, MA, USA. [4]Department of Land, Air, and Water Resources, University of California, Davis, Davis, CA, USA. [5]Environmental Sciences Division, Oak Ridge National Laboratory, Oak Ridge, TN, USA.

*Address correspondence to: xxu@sdsu.edu

Citation: Wang Y, He L, Liu J, Arndt KA, Mazza Rodrigues JL, Zona D, Lipson DA, Oechel WC, Ricciuto DM, Wullschleger SD, et al. Intensified Positive Arctic–Methane Feedback under IPCC Climate Scenarios in the 21st Century. *Ecosyst. Health Sustain.* 2024;10:Article 0185. https://doi.org/10.34133/ehs.0185

Submitted 5 September 2023
Accepted 23 March 2024
Published 17 April 2024

The positive Arctic–methane (CH_4) feedback forms when more CH_4 is released from the Arctic tundra to warm the climate, further stimulating the Arctic to emit CH_4. This study utilized the CLM-Microbe model to project CH_4 emissions across five distinct Arctic tundra ecosystems on the Alaska North Slope, considering three Shared Socioeconomic Pathway (SSP) scenarios using climate data from three climate models from 2016 to 2100. Employing a hyper-resolution of 5 m × 5 m within 40,000 m^2 domains accounted for the Arctic tundra's high spatial heterogeneity; three sites were near Utqiaġvik (US-Beo, US-Bes, and US-Brw), with one each in Atqasuk (US-Atq) and Ivotuk (US-Ivo). Simulated CH_4 emissions substantially increased by a factor of 5.3 to 7.5 under the SSP5–8.5 scenario compared to the SSP1–2.6 and SSP2–4.5 scenarios. The projected CH_4 emissions exhibited a stronger response to rising temperature under the SSP5–8.5 scenario than under the SSP1–2.6 and SSP2–4.5 scenarios, primarily due to strong temperature dependence and the enhanced precipitation-induced expansion of anoxic conditions that promoted methanogenesis. The CH_4 transport via ebullition and plant-mediated transport is projected to increase under all three SSP scenarios, and ebullition dominated CH_4 transport by 2100 across five sites. Projected CH_4 emissions varied in temperature sensitivity, with a Q_{10} range of 2.7 to 60.9 under SSP1–2.6, 3.8 to 17.6 under SSP2–4.5, and 5.7 to 17.2 under SSP5–8.5. Compared with the other three sites, US-Atq and US-Ivo were estimated to have greater increases in CH_4 emissions due to warmer temperatures and higher precipitation. The fact that warmer sites and warmer climate scenarios had higher CH_4 emissions suggests an intensified positive Arctic–CH_4 feedback in the 21st century. Microbial physiology and substrate availability dominated the enhanced CH_4 production. The simulated intensified positive feedback underscores the urgent need for a more mechanistic understanding of CH_4 dynamics and the development of strategies to mitigate CH_4 across the Arctic.

Introduction

Methane (CH_4) is a potent greenhouse gas in the atmosphere [1,2]. The concentration of CH_4 in the atmosphere has begun to rise again since 2007 and showed a big jump in 2021–2022, leading to an annual average CH_4 concentration of 1,900 parts per billion (ppb) in 2022 [3,4]. Arctic soils are considered a substantial net source of atmospheric CH_4 and have the potential to release massive CH_4 fluxes due to the rich carbon (C) stocks and expansion of inundated soils under climate changes [5,6]. Arctic CH_4 emissions are estimated to be 15 to 50 Tg CH_4 $year^{-1}$, accounting for 20 to 25% of global natural CH_4 emissions [7]. Process-based biochemistry models predicted that Arctic CH_4 emissions will be two to three times greater by 2100 due to warming [8,9]. In addition, Oh *et al.* [5] reported a 70 to 100% increase in wetland CH_4 emissions by 2100 under the Representative Concentration Pathways (RCPs) of 8.5 W m^{-2}. This undoubtedly emphasizes the importance of CH_4 projections in the Arctic for the next few decades.

Arctic regions have been warming two to four times faster than the global average in recent decades [10,11]. Air temperature in the Arctic has increased and could continue to increase by more than 10 °C by 2100 relative to present day [1]. Field experiments in the Arctic found that warming could have no

effect or increase CH_4 fluxes by 15 to 550% depending on changes in water table and vegetation growth [12]. For example, data-constrained projections showed a 400% increase in CH_4 emissions under 9 °C warming at a temperate peatland [13]. However, large uncertainties still exist in predicting responses of Arctic CH_4 fluxes to future climate change due to implicit representation of methanogenesis and methanotroph [2,14], even though CH_4 production and emission processes have been extensively explored [15,16].

The CLM-Microbe model takes advantage of a new microbial functional group-based CH_4 module [6,14,17,18] and a new framework for microbial control on C mineralization [19–21] in the default decomposition subroutines in CLM4.5 [22,23]. It allows for a better understanding of the mechanisms and dynamics of CH_4 production, oxidation, and transport pathways under climate change. Our previous studies have validated this module with incubation and closed-chamber fluxes [14,18]. In addition, CH_4 fluxes have been upscaled from the plot level to landscape scales using different footprint algorithms, consistent with eddy covariance (EC) fluxes in Alaskan tundra ecosystems [6,14]. CH_4 emissions have been well studied using the CLM-Microbe model regarding spatial heterogeneities in vegetation, soil hydrology, and topography [6,14,24]. Therefore, the CLM-Microbe model could help us to understand the mechanisms of future CH_4 dynamics through each CH_4 process at the landscape scales in the Arctic tundra. However, this model has not been tested for future CH_4 projection under different climate scenarios.

This study continued our research on simulating CH_4 fluxes in the Arctic and further estimated how future Arctic CH_4 fluxes change under climate change. In this study, we applied the CLM-Microbe model to project CH_4 fluxes from 2016 to 2100 under SSP1–2.6, SSP2–4.5, and SSP5–8.5 scenarios derived from three climate models for five Alaskan tundra ecosystems. We aim to (a) project how Arctic CH_4 emissions will change under different Shared Socioeconomic Pathway (SSP) scenarios by 2100, (b) understand the mechanisms behind future CH_4 dynamics under different SSP scenarios, and (c) investigate the differences of projected future CH_4 fluxes across different Alaskan tundra ecosystems. This effort fills the gap in mechanistic understanding and predicting CH_4 cycling in the Arctic under future climate scenarios.

Materials and Methods

Site information

We performed model experiments at five sites in the northern Alaskan tundra; detailed information is available in [15,25]. Three of these sites are located in Utqiaġvik (referred to as Utqiaġvik sites), including US-Beo (71.2810°N, 156.6124°W), US-Bes (71.2809°N, 156.5965°W), and US-Brw (71.3225°N, 156.6093°W) [26]. US-Beo is a polygonal coastal tundra site on the Barrow Environmental Observatory, and US-Bes is an inundated wet coastal tundra site at the southern end of the previous Biocomplexity Experiment, usually with a water table above the surface of the soil due to its low elevation. US-Brw is a well-drained, moist coastal tundra site, and its vegetation is dominated by graminoids. Another two sites are US-Atq (70.4696°N, 157.4089°W) in Atqasuk, AK, which is located about 100 km south of Utqiaġvik, and US-Ivo (68.4805°N, 155.7569°W) in Ivotuk, AK, which is located approximately 300 km south of Utqiaġvik in the northern foothills of the Brooks Range [27]. US-Atq is characterized by polygonized tussock tundra and sandy soils [28], and US-Ivo, the most inland site, has the warmest annual temperature and lies on gently sloping tussock tundra [27]. These study sites have a polar maritime climate, with most precipitation falling during the summer months (June to August). Detailed meteorological and vegetation information on these sites is posted in the Oak Ridge National Laboratory Distributed Active Archive Center (ORNL DAAC) (https://doi.org/10.3334/ORNLDAAC/1562 and https://doi.org/10.3334/ORNLDAAC/1546) and in [27].

Description of the CH_4 module

The CLM-Microbe model branches from the framework of default CLM 4.5 developed in 2013 [22,23]. Improvements in the CLM-Microbe model include a microbial functional group-based CH_4 module [14,18] and a new framework for microbial controls on C mineralization [19–21]. This model has been verified for simulating CH_4 fluxes among different microtopographic types and applied for upscaling from the plot level to EC tower domain in the Alaskan Arctic tundra ecosystems [6,14]. Detailed mathematical expressions and default parameter settings for CH_4 production, oxidation, and transport (i.e., diffusion, ebullition, and plant-mediated transport) processes can be obtained from [14,18]. The code for the CLM-Microbe model is archived at https://github.com/email-clm/clm-microbe. The model version used in this study was obtained from GitHub on 2020 May 27 [29].

SSP scenarios

The Coupled Model Intercomparison Project Phase 6 (CMIP6) includes future warming projections for the 21st-century climate with different SSP scenarios. Compared to the RCPs, five main SSPs (SSP1–1.9, SSP1–2.6, SSP2–4.5, SSP3–7.0, and SSP5–8.5) are more evenly spaced and extend to lower 2100 radiative forcing and temperatures [30]. In this study, we chose SSP1–2.6, SSP2–4.5, and SSP5–8.5 from CMIP6, which allowed us to explore the impact of different magnitudes of anthropogenic forcing and the response of the climate system simulated with varying representations of the model [31]. SSP1–2.6 is the "2 °C scenario" of the "sustainability" SSP1 socioeconomic family, whose nameplate 2100 radiative forcing level is 2.6 W m^{-2}. This SSP1–2.6 scenario corresponds to the previous scenario generation RCP-2.6 [30]. SSP2–4.5 is of the "middle of the road" socioeconomic family SSP2 with a nominal 4.5 W m^{-2} radiative forcing level by 2100—approximately corresponding to the RCP-4.5 scenario [30]. SSP5–8.5 marks the upper edge of the SSP scenario spectrum with a high reference scenario in a high fossil fuel development world throughout the 21st century [30].

Climate models and CLM-Microbe forcing data

Three climate models in CMIP6 were selected to retrieve data for these SSP scenarios from 2016 to 2100, as they are very representative and widely used worldwide and include all variables at the daily time step required by the CLM-Microbe model. (a) BCC-CSM2-MR is a medium-resolution version of the BCC-CSM (T106 in the atmosphere and 1° latitude × 1° longitude in the ocean), which is the baseline for BCC participation in CMIP6 (https://esgf-node.llnl.gov/search/cmip6/). (b) The CESM version 2 (CESM2) is the latest generation of the Community Earth System model. The output fields from previous CESM2 simulations have been posted on the Earth

System Grid Federation (ESGF; https://esgf-node.llnl.gov/search/cmip6/). (c) EC-Earth3 is the latest version of EC-Earth in CMIP6 that utilizes the original idea of a climate model system based on the seasonal prediction system of the European Centre for Medium-Range Weather Forecasts (ECMWF) (https://esgf-node.llnl.gov/search/cmip6/). The required meteorological variables for model simulations are total incident solar radiation, incident longwave radiation, total precipitation, surface air pressure, specific humidity, air temperature, and wind speed. Climate data were calibrated by trends of future data and offsets between historical and future data and then validated based on historical data (Figs. S1, S4, and S5). The model forcing data for the historical runs were adopted from CRUNCEP, which is consistent with our previous model simulations [6]. Detailed information for meteorological variables of each climate model corresponding to variables of CRUNCEP is shown in Tables S1 to S3.

Additional forcing data included the spatial distribution of vegetation and a digital elevation model (DEM) with a resolution of 4 m covering the tower domain at each site and soil organic carbon (SOC) concentration at the top 10 soil layers defined in CLM4.5 [22,23]. Vegetation distribution for Utqiaġvik sites was determined using a random forest algorithm using the plant functional type from [32] as training data. For the US-Atq and US-Ivo sites, an unsupervised linear spectral unmixing was performed in ENVI V5.2 (L3Harris Geospatial) using the vegetation classes from a previous publication [27], with an additional open water category. Four plant species across five areas were classified into model-defined PFTs (plant functional types), including Arctic C3 grass, bare soil, broadleaf evergreen shrub, and deciduous boreal shrub. Averages of plant cover at US-Beo, US-Bes, US-Brw, US-Atq, and US-Ivo sites were 88%, 82%, 91%, 73%, and 78%, respectively; US-Ivo had larger proportions of shrubs than other sites [6]. A vegetation distribution map of the five study sites was available in [6]. A 0.5-m (vertical resolution) DEM was used for elevation data at Utqiaġvik sites [33]. Elevation maps for US-Atq and US-Ivo were downloaded from ArcticDEM (v3.0 Pan-Arctic) with a spatial resolution of 2 m based on the geographic information of these two sites [34] and further processed to maps with a spatial resolution of 4 m using MATLAB software (R2018a, the MathWorks). SOC concentrations at 0 to 10, 10 to 20, 20 to 30, and 30 to 40 cm at US-Bes, US-Atq, and US-Ivo were derived from the Northern Circumpolar Soil Carbon Database [35]. Due to the lack of SOC data, we assumed that US-Beo and US-Brw had the same SOC distribution with US-Bes since these sites are adjacent, which might affect the accuracy of CH_4 projection for these two sites. Detailed calculation processes can be found in [6].

Model implementation under three SSP scenarios

Model implementation for historical simulation was carried out in three stages, similar to the default CLM4.5 protocols [36]. The first phase is an accelerated model spin-up; we set the accelerated model spin-up for 2,000 years to allow more C accumulation, as the Arctic tundra has a low rate and long period of C sequestration. Then, a final spin-up was set up for 50 years to allow the modeled system to reach a steady state. After the final spin-up, the transient simulation was set up to cover the period of 1850–2015 for all five sites with the observed climate and soil data. For each site, one model run was conducted in an area of 200 m × 200 m with the EC tower as the center at a spatial resolution of 4 m, covering 2,500 grid cells. Detailed information for historical simulation is available in [6].

From 2016 to 2100, we reset the transient simulation to accomplish CH_4 projections with three climate datasets under each of the SSP1–2.6, SSP2–4.5, and SSP5–8.5 scenarios. All parameter values were kept consistent with previous studies [6,18], and the same model parameters and settings were applied to all five sites under different SSP scenarios. Thus, we conducted nine model runs at a half-hour time step for each study site for 85 years. Detailed information on site and parameter setup can be derived from [6].

Temperature sensitivity for CH_4 flux

Temperature dependence of CH_4 cycling is a critical parameter for quantifying the warming impacts on individual CH_4 processes and the net flux, and it is generally termed as Q_{10}, defined as the change in a reaction rate when temperature increases by 10 °C [37]. Intrinsic Q_{10} is defined as the increases in methanogenesis or methanotrophy under 10 °C warming when other biotic and abiotic factors were excluded; apparent Q_{10} is defined as increases in CH_4 processes when temperature increases by 10 °C along with alterations of other abiotic and biotic factors [37]. Intrinsic Q_{10} is used as a theoretic parameter for individual CH_4 processes in models [18], while the apparent Q_{10} can quantify the temperature sensitivity of ecosystem-level CH_4 flux [38].

To analyze the temperature sensitivity of CH_4 fluxes, we calculated the apparent Q_{10} coefficient as the measure of the change rates of CH_4 flux as a consequence of the temperature increment of 10 °C [37]. We used the linear regression to estimate the Q_{10} coefficient with datasets of CH_4 fluxes under one SSP scenario using one climate model ($n = 85$). The formula for estimating the Q_{10} was as follows:

$$\log_{10}\left(\frac{R}{R_0}\right) = \frac{T - T_0}{10} \times a + b \quad (1)$$

where R is the CH_4 flux (gC m^{-2} $year^{-1}$) at temperature T (°C) and R_0 is the CH_4 flux (gC m^{-2} $year^{-1}$) at temperature T_0 (°C) in 2016. Q_{10} is estimated as 10 to the power of the coefficient a, and the coefficient b is the estimated intercept. It should be noted that the calculated Q_{10} is an apparent term, which is affected by a mixture of many environmental factors and the intrinsic Q_{10}—a key factor for each of the CH_4 processes represented in the CLM-Microbe model [14,18].

Statistical analysis

Dynamics of annual CH_4 fluxes, air temperature, precipitation, soil temperature, soil moisture, net primary production (NPP), and canopy evapotranspiration (ET) during 2016–2100 were plotted for five sites under different SSP scenarios based on three climate models using R (R Core Team, 2020). Averages and standard deviations of CH_4 fluxes in 2006–2015, 2016–2025, 2050–2059 (2050s), and 2090–2099 (2090s) were also calculated under three SSP scenarios. One-way analysis of variance (ANOVA) and the Duncan test were employed to assess the differences in CH_4 fluxes among different periods for each site and among different sites for each period. Before this analysis, the data were tested and followed the assumptions of ANOVA. Changing rates of CH_4 fluxes, each CH_4 process, and each environmental factor in 2016–2100 were calculated by the general linear regression analysis using all model output based on three climatic datasets for each study site under each SSP scenario. Contributions of three CH_4 transport pathways to CH_4 fluxes, including diffusion,

ebullition, and plant-mediated transport, were displayed for each study site under different SSP scenarios. Partial correlation analyses between CH_4 emissions and each CH_4 process and environmental factor were done for each site under to quantify the contributions of all biological and environmental factors. All statistical analyses and plots were made using R [39].

Results

Projected CH_4 fluxes during 2016–2100 under different SSP scenarios

Projected CH_4 emissions increase during 2016–2100 under the three SSP scenarios with different change rates among five study sites (Fig. 1 and Fig. S2). Especially after the 2050s, CH_4 fluxes drastically increase under SSP5–8.5 compared with SSP1–2.6 and SSP2–4.5 (Fig. 1). Until 2100, projected CH_4 fluxes under SSP5–8.5 were four- to sevenfold higher than those under SSP1–2.6 and SSP2–4.5 (Fig. 1F to J). There are no substantial differences in projected CH_4 fluxes between SSP1–2.6 and SSP2–4.5 (Fig. 1F to J), although the fluxes under SSP2–4.5 seemed slightly higher (less than 40%) than under SSP1–2.6 after the 2050s (Fig. 1A to E). In the 2090s, projected CH_4 fluxes increase by 0.39 to 1.21 under SSP1–2.6 and SSP2–4.5 but increase by a factor of 5.3 to 7.5 under SSP5–8.5 among five sites in Arctic tundra (Fig. 1).

Projected average CH_4 fluxes (unit: gC m^{-2} $year^{-1}$) during 2016–2025 are comparable to that in the 2050s under different SSP scenarios, which are 2.47 ± 0.10 gC m^{-2} $year^{-1}$ at US-Beo, 2.15 ± 0.09 gC m^{-2} $year^{-1}$ at US-Bes, 2.56 ± 0.11 gC m^{-2} $year^{-1}$ at US-Brw, 3.67 ± 0.19 gC m^{-2} $year^{-1}$ at US-Atq, and 3.89 ± 0.20 gC m^{-2} $year^{-1}$ at US-Ivo (Fig. 1F to J). Moreover, they are comparable with historical fluxes during 2006–2015 as simulated by the CLM-Microbe model (Fig. 1F to J) [6]. Additionally, projected CH_4 fluxes in the warmer study sites of US-Atq and US-Ivo exhibit larger absolute increments than at US-Beo, US-Bes, and US-Brw (Fig. 1F to J). For example, projected CH_4 fluxes in the 2090s under SSP5–8.5 are around 20 gC m^{-2} $year^{-1}$ at US-Beo, US-Bes, and US-Brw, whereas fluxes approach 30 gC m^{-2} $year^{-1}$ at US-Atq and US-Ivo.

Changes of CH_4 processes and climate factors under three SSP scenarios

Conceptual models of CH_4 processes are developed for each study site under different SSP scenarios, illustrating change rates of each CH_4 process [i.e., fermentation of soil organic matter (SOM)/dissolved organic carbon (DOC) to acetate, acetoclastic methanogenesis, hydrogenotrophic methanogenesis, diffusion, ebullition, the plant-mediated transport, aerobic oxidation, and anaerobic oxidation], climate factors (i.e., air temperature, soil temperature, precipitation, and soil moisture), vegetation factor (i.e., NPP), and soil factors (i.e., concentrations of DOC, acetate, and CH_4) (Fig. 2 and Table). Overall, all CH_4 processes except anaerobic oxidation are enhanced (Fig. 2 and Table S5) and all vegetation, soil, and climate factors are increased during 2016–2100 (Fig. 2, Table, and Table S5). Moreover, change rates of all CH_4 processes, vegetation, soil factors (except DOC), and climate factors are larger under SSP5–8.5 than under SSP1–2.6 and SSP2–4.5 (Fig. 2, Figs. S1 to S3, and Table). Under different SSP scenarios, air temperature increases by 0.02 to 0.13 °C $year^{-1}$, whereas soil temperature (at 10 cm) has similar increments with air temperature, ranging from 0.015 to 0.148 °C $year^{-1}$ (Table). Change rates of air temperature and soil temperature under SSP2–4.5 and SSP5–8.5 are approximately 2.6 and 5.7 times

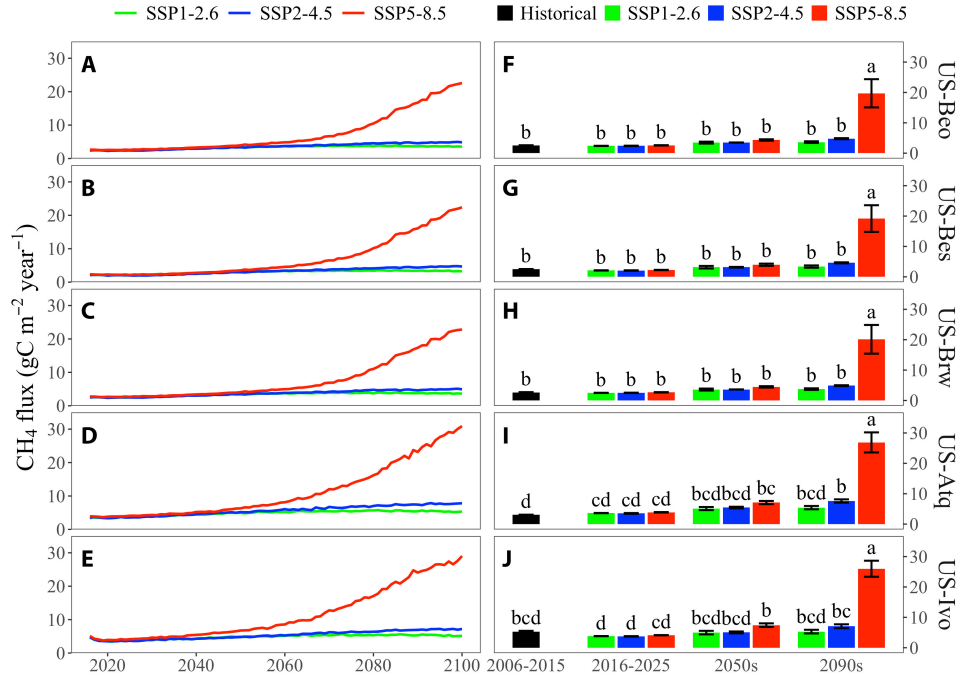

Fig. 1. Projections of CH_4 fluxes at (A) US-Beo, (B) US-Bes, (C) US-Brw, (D) US-Atq, and (E) US-Ivo during 2016–2100 under different Shared Socioeconomic Pathways (SSP) scenarios. The bar charts show projected CH_4 fluxes (mean ± SD; $n = 10$ or 30) for the periods of 2006–2015, 2016–2025, the 2050s, and 2090s at (F) US-Beo, (G) US-Bes, (H) US-Brw, (I) US-Atq, and (J) US-Ivo under SSP1–2.6, SSP2–4.5, and SSP5–8.5 scenarios. Green indicates the SSP1–2.6 scenario, blue indicates the SSP2–4.5 scenario, red indicates the SSP5–8.5 scenario, and black indicates the historical fluxes of 2006–2015 simulated by the CLM-Microbe model. Error bars represent the standard deviation; different letters above error bars indicate significant differences at the level of $P = 0.05$ (ANOVA and Duncan's multiple range test) among different periods and SSP scenarios at each site.

greater than that under SSP1–2.6 among five sites except US-Ivo (Table). Precipitation increased by 0.362 to 0.606 mm year^{-1} under SSP1–2.6 and SSP2–4.5 but increase by 0.828 to 1.861 mm year^{-1} under SSP5–8.5 (Table). Soil moisture (at 10 cm) increased by 0.059 to 0.225% year^{-1} (Table). Additionally, change rates of precipitation and soil moisture under SSP2–4.5 were 1.2 to 1.4 times and 1.3 to 2.2 times higher than that under SSP1–2.6, respectively, whereas change rates of precipitation and soil moisture under SSP5–8.5 were 2.3 to 4.1 times and 1.9 to 2.9 times greater than that under SSP1–2.6, respectively (Table).

Different CH_4 processes show dissimilar contributions to CH_4 fluxes under different SSP scenarios but mutually strengthen total CH_4 fluxes. Generally, the increase or decrease is larger under SSP5–8.5 than under SSP2–4.5 and SSP1–2.6 (Fig. 2 and Table S5). For example, at US-Beo, NPP increases more under warmer scenarios, with a rise of 2.275, 3.194, and 5.776 gC m^{-2} year^{-1} under SSP1–2.6, SSP2–4.5, and SSP5–8.5, respectively. However, soil DOC increases more under less warm scenarios, 0.445, 0.387, and 0.321 gC m^{-2} year^{-1} under SSP1–2.6, SSP2–4.5, and SSP5–8.5, respectively (Fig. 2A). More SOM/DOC is fermented to acetate under warmer scenarios, and this process is significantly strengthened under SSP5–8.5 (0.025 gC m^{-2} year^{-1}) compared with SSP1–2.6 (0.004 gC m^{-2} year^{-1}) and SSP2–4.5 (0.007 gC m^{-2} year^{-1}) (Fig. 2A) ($P < 0.01$). Acetate concentrations are increased more under warmer scenarios, with a substantial increase of 0.031 gC m^{-2} year^{-1} under the SSP5–8.5 scenario (Fig. 2A). Acetoclastic methanogenesis is enhanced, with an increase of 0.005, 0.011, and 0.090 gC m^{-2}

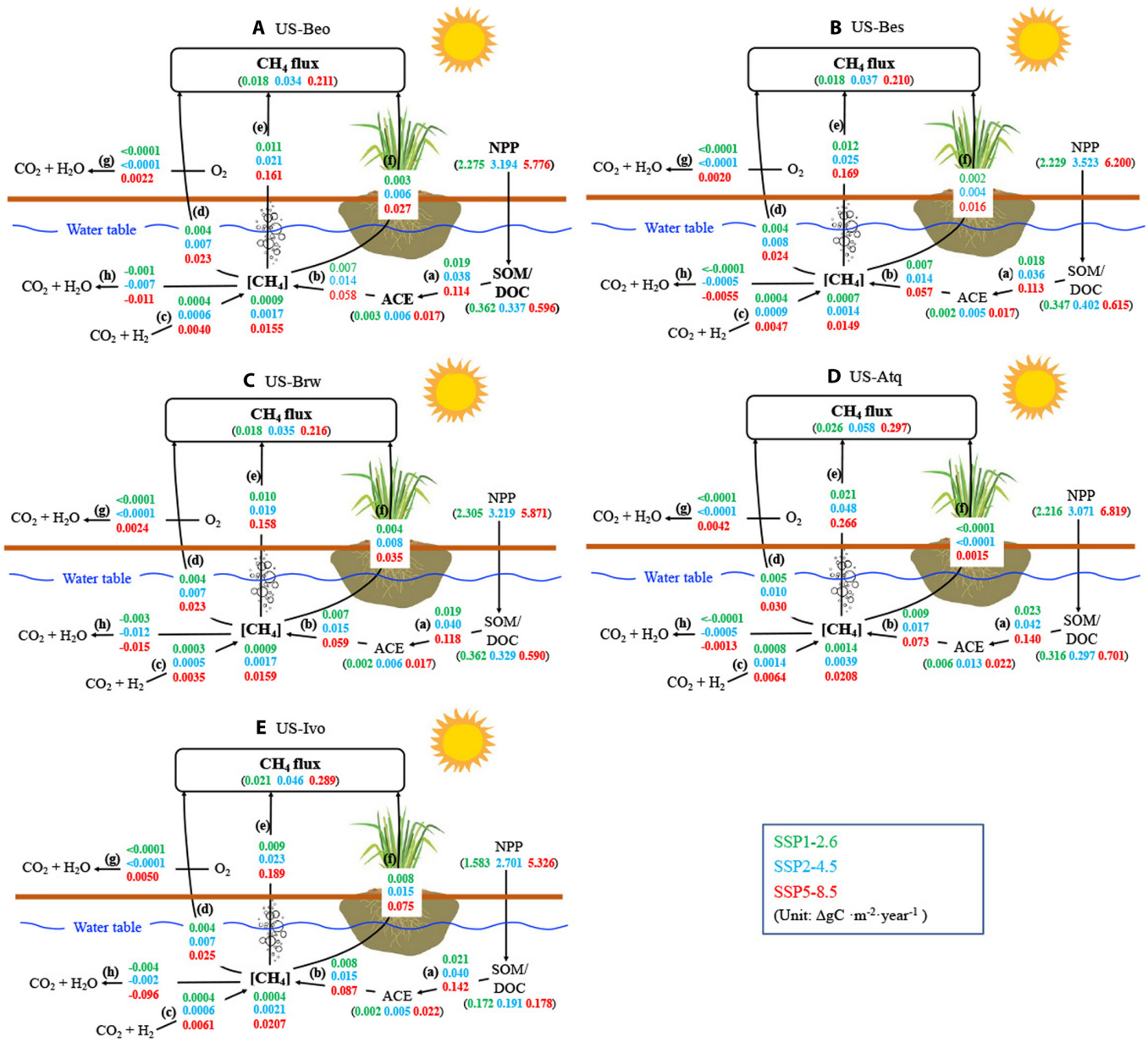

Fig. 2. Conceptual model of changes in CH_4 processes at (A) US-Beo, (B) US-Bes, (C) US-Brw, (D) US-Atq, and (E) US-Ivo under different SSP scenarios. CH_4 processes (unit: ΔgC m^{-2} year^{-1}) include (a) fermentation of soil organic matter (SOM)/dissolved organic carbon (DOC) to acetate, (b) acetoclastic methanogenesis, (c) hydrogenotrophic methanogenesis, (d) diffusion, (e) ebullition, (f) the plant-mediated transport, (g) aerobic oxidation, and (h) anaerobic oxidation of CH_4. Vegetation factor is net primary production (NPP; ΔgC m^{-2} year^{-1}), and soil factors include soil DOC concentration ([DOC], ΔgC m^{-2} year^{-1}), acetate concentration ([ACE], ΔgC m^{-2} year^{-1}), and CH_4 concentration ([CH_4], ΔgC m^{-2} year^{-1}). The numbers in the conceptual model and table are the changing rates of each process and factor during 2016–2100.

Table 1. Annual changes of air temperature, precipitation, soil temperature, and soil moisture at top 10-cm soil depth at US-Beo, US-Bes, US-Brw, US-Atq, and US-Ivo under SSP1–2.6, SSP2–4.5, and SSP5–8.5 scenarios

Variable	Site	SSP1–2.6	SSP2–4.5	SSP5–8.5
Air temperature (Δ°C year^{-1})	US-Beo	0.023	0.059	0.130
	US-Bes	0.023	0.059	0.130
	US-Brw	0.023	0.059	0.130
	US-Atq	0.021	0.054	0.123
	US-Ivo	0.020	0.042	0.102
Precipitation (Δmm year^{-1})	US-Beo	0.362	0.440	0.828
	US-Bes	0.362	0.440	0.828
	US-Brw	0.362	0.440	0.828
	US-Atq	0.446	0.606	1.366
	US-Ivo	0.454	0.594	1.861
Soil temperature (Δ°C year^{-1})	US-Beo	0.024	0.066	0.138
	US-Bes	0.023	0.064	0.135
	US-Brw	0.024	0.066	0.138
	US-Atq	0.023	0.054	0.125
	US-Ivo	0.015	0.045	0.148
Soil moisture (Δ% year^{-1})	US-Beo	0.085	0.175	0.199
	US-Bes	0.077	0.140	0.225
	US-Brw	0.085	0.184	0.209
	US-Atq	0.078	0.099	0.150
	US-Ivo	0.059	0.107	0.163

year^{-1} under SSP1–2.6, SSP2–4.5, and SSP5–8.5, respectively (Fig. 2A). Hydrogenotrophic methanogenesis is also raised by 0.0004, 0.0007, and 0.0074 gC m^{-2} year^{-1} under SSP1–2.6, SSP2–4.5, and SSP5–8.5, respectively, but their increments are much lower than acetoclastic methanogenesis (Fig. 2A). All transport pathways are promoted under climate scenarios, especially the ebullition pathway (Fig. 2A). Specifically, ebullition increase by 0.011, 0.021, and 0.161 gC m^{-2} year^{-1} under SSP1–2.6, SSP2–4.5, and SSP5–8.5, respectively, which is about three to seven times higher than other transport pathways (Fig. 2A). CH_4 oxidation changes little compared with the production and transport of CH_4, and their changes are so small that they could be ignored under SSP1–2.6 and SSP2–4.5 (Fig. 2A). Anaerobic and aerobic oxidations enhance by 0.0131 and 0.0016 gC m^{-2} year^{-1} under SSP5–8.5, respectively (Fig. 2A). Of those CH_4 processes, CH_4 production and transport mainly determine CH_4 fluxes. In total, CH_4 fluxes increase by 0.018, 0.034, and 0.211 gC m^{-2} year^{-1} under SSP1–2.6, SSP2–4.5, and SSP5–8.5, respectively (Fig. 2A). The same conceptual models built for other study sites can be interpreted in the same manner as US-Beo.

Changes in CH_4 processes and climate factors among five study sites

Three sites close to Utqiaġvik have the same values and increases in air temperature and precipitation with comparable increments of soil temperature (0.023 to 0.138 °C year^{-1}) and moisture (0.077 to 0.225 mm year^{-1}) due to their close locations, which were distinct from US-Atq and US-Ivo (Table 1 and Figs. S1, S5, and S6). Under similar climate conditions, the increase of CH_4 fluxes is comparable, 0.018, 0.035, and 0.212 gC m^{-2} year^{-1} under SSP1–2.6, SSP2–4.5, and SSP5–8.5, respectively (Fig. 2A to C). Comparing these three sites, <18% differences in change rates at US-Bes and US-Brw than US-Beo are found in NPP, soil DOC and CH_4 concentration, fermentation of SOM/DOC to acetate, acetoclastic and hydrogenotrophic methanogenesis, aerobic oxidation and diffusion, and ebullition (Fig. 2A to C). Changes of anaerobic oxidation vary among Utqiaġvik sites, but its contribution to CH_4 flux can be ignored due to its small magnitudes among all CH_4 processes (Fig. 2A to C). Change rates of the plant-mediated transport at US-Bes were 40% lower and at US-Brw were 30% greater than at US-Beo under three SSP scenarios (Fig. 2A to C). Of three CH_4 transport pathways, ebullition contributes more to the increase of CH_4 fluxes among Utqiaġvik sites (Fig. 2A to C). US-Bes has a greater increase in ebullition and smaller change in plant-mediated transport than US-Beo, whereas US-Brw has a smaller increase in ebullition but larger increase in plant-mediated transport than US-Beo (Fig. 2A to C).

US-Atq shows a greater rise of precipitation but lower increases in air temperature, soil temperature, and moisture than Utqiaġvik sites (Table 1). But it has the greatest increase of CH_4 fluxes across all five sites with 0.026, 0.058, and 0.297 gC m^{-2} year^{-1} under SSP1–2.6, SSP2–4.5, and SSP5–8.5, respectively (Fig. 2D and Table 1). Additionally, US-Atq displays similar increases in NPP but a little smaller increase in soil DOC concentration (Fig. 2A to D). Soil CH_4 and acetate concentrations at US-Atq were 1.4 to 4.5 times higher than that at US-Beo (Fig. 2A and D). Moreover, increases in its CH_4 production,

oxidation, and transport processes except the plant-mediated transport and anaerobic oxidation are much larger than US-Beo under all SSP scenarios (Fig. 2A and D). Acetoclastic methanogenesis is accelerated more among production and oxidation processes, with 0.008, 0.019, and 0.128 gC m^{-2} $year^{-1}$ under SSP1–2.6, SSP2–4.5, and SSP5–8.5, respectively (Fig. 2D). Changes in CH_4 oxidation could be ignored due to their relatively small values and changes under three SSP scenarios, although aerobic and anaerobic oxidation is increased by 0.025 and 0.008 gC m^{-2} $year^{-1}$ under SSP5–8.5, respectively (Fig. 2D). In addition, the plant-mediated transport is the smallest and shows little changes at US-Atq (Fig. 2 and Table S5). Both diffusion and ebullition are accelerated, but ebullition shows the largest increase among all five sites with annual values of 0.021, 0.048, and 0.266 gC m^{-2} $year^{-1}$ under SSP1–2.6, SSP2–4.5, and SSP5–8.5, respectively (Fig. 2D).

With relatively lower air temperature and higher precipitation among five sites (Fig. S1), US-Ivo also has lower rises in air temperature and greater increases in precipitation (Table 1). Its changes of soil temperature are still lower under SSP1–2.6 and SSP2–4.5 but is the greatest under SSP5–8.5 among five sites (Table 1). But soil moisture at US-Ivo shows relatively lower increases even with greater increases in precipitation compared with other sites (Table 1). US-Ivo displays an increase of CH_4 fluxes by 0.021 and 0.058 gC m^{-2} $year^{-1}$ under SSP1–2.6 and SSP2–4.5, which were lower than US-Atq but higher than Utqiaġvik sites (Fig. 2). The increases of NPP and soil DOC concentration are much smaller than other sites under all SSP scenarios (Fig. 2E). CH_4 production processes increase more than Utqiaġvik sites but less than US-Atq, with the increases of 0.006, 0.014, and 0.143 gC m^{-2} $year^{-1}$ in acetoclastic methanogenesis and 0.0004, 0.001, and 0.0117 gC m^{-2} $year^{-1}$ in hydrogenotrophic methanogenesis (Fig. 2). CH_4 oxidation can also be ignored among all CH_4 processes, with a relatively high increase of 0.0032 and 0.03 gC m^{-2} $year^{-1}$ in anaerobic and aerobic oxidation (Fig. 2E). Diffusion and ebullition show comparable increases with Utqiaġvik sites, whereas the plant-mediated transport had the largest increases compared with other sites (Fig. 2).

Changes in three CH_4 transport pathways under different SSP scenarios

Of all CH_4 processes, three transport pathways regulate the increasing CH_4 fluxes among the five sites, even with contrasting changes in CH_4 production and oxidation processes under different SSP scenarios. Overall, the contribution rates of the three transport pathways are similar during 2016–2025 and 2050s among different SSP scenarios but differ in the 2090s (Figs. 3 and 4 and Fig. S9). The contributions of plant-mediated transport and ebullition to CH_4 transport increased, whereas the contribution of diffusion decreased over time across five sites under different SSP scenarios. Until 2100, ebullition dominates CH_4 transport across all sites under all SSP scenarios (Fig. 4).

During 2016–2025, diffusion dominates CH_4 transport at US-Beo, US-Bes, and US-Brw, contributing approximately half of total CH_4 fluxes for all SSP scenarios (Fig. 3). Ebullition contributes about 40% of CH_4 fluxes across the three sites, whereas plant-mediated transport contributes about 8.5% at US-Beo, 4% at US-Bes, and 11.5% at US-Brw (Fig. 3). At US-Atq, ebullition contributes about 59% of total CH_4 fluxes, whereas the contribution of plant-mediated transport can be ignored under all SSP scenarios (Fig. 3D, I, and N). Diffusion also contributes substantial CH_4 fluxes at US-Ivo, but all three transport pathways contribute more comparable CH_4 fluxes, ~41% from diffusion, ~35% from ebullition, and ~24% via plants (Fig. 3E, J, and O).

By 2050s, the contribution of CH_4 transport from diffusion decreases, whereas the plant-mediated transport and ebullition increase across five sites under all SSP scenarios (Fig. S9). In the 2090s, both plant-mediated transport and ebullition continue to increase under all SSP scenarios, but their contribution ratios somewhat change compared to the 2050s for SSP1–2.6 and SSP2–4.5 (Fig. 4). However, under SSP5–8.5, ebullition increases to 72.7% at US-Beo, 77.1% at US-Bes, 69.5% at US-Brw, 85.7% at US-Atq, and 61.5% at US-Ivo by 2090s (Fig. 4K to O). At US-Beo, US-Bes, and US-Brw, diffusion contributes about 42% of total CH_4 fluxes under SSP1–2.6 and 37% under SSP2–4.5 (Fig. 4). The plant-mediated transport could be ignored at US-Atq as it contributes less than 0.5% for all SSP scenarios (Fig. 4D, I, and N). However, it contributes the largest at US-Ivo among five sites, with approximately 27% under all SSP scenarios (Fig. 4E, J, and O).

Temperature sensitivity for CH_4 flux under different SSP scenarios

The Q_{10} values for CH_4 flux vary among SSP scenarios, with a lower value with BCC-CSM2-MR and a relatively higher value with CESM2 and EC-Earth3 (Fig. 5). The Q_{10} range is 2.7 to 9.8 using BCC-CSM2-MR, 7.1 to 17.6 with CESM2, and 5 to 60.9 with EC-Earth3 (Fig. 5). Using EC-Earth3, Q_{10} has extremely high values under SSP1–2.6, ranging from 18.4 at US-Ivo to 60.9 at US-Bes; however, Q_{10} is lower under SSP2–4.5 than under SSP5–8.5 (Fig. 5). Q_{10} increases along the gradient of SSP1–2.6, SSP2–4.5, and SSP5–8.5 at US-Bes, US-Atq, and US-Ivo using BCC-CSM2-MR, whereas there are no obvious trends for Q_{10} along such scenario gradient using the other climate models across all five sites (Fig. 5). US-Beo and US-Brw have comparable Q_{10} values for the different SSP scenarios with each climate model.

Discussion

Mechanisms of future CH_4 emissions under different SSP scenarios

Future CH_4 emissions have been projected to gradually increase under different SSP scenarios. Our results show that at northern high-latitude regions, as air temperature increases by 1 to 2 °C under SSP1–2.6, 3 to 5 °C under SSP2–4.5, and 7 to 12 °C under SSP5–8.5, an increase of 39 to 60%, 89 to 121%, and 531 to 751% in CH_4 emissions occurs under SSP1–2.6, SSP2–4.5, and SSP5–8.5, respectively (Figs. S4 and S5). This confirms that warmer temperatures ($r_p = 0.832$, $P < 0.05$; Fig. S10) and more precipitation ($r_p = 0.696$, $P < 0.05$; Fig. S10) could enhance CH_4 emissions, which is consistent with previous studies [13,40]. In addition, previous studies reported that a 3 to 5 °C warming more than doubled the boreal CH_4 emissions [41], and a ~5 °C warming tripled northern Alaskan emissions in the midsummer. Ma *et al.* [13] showed that modeled CH_4 emissions increased by 30%, 100%, 275%, and 400% under 2.25, 4.5, 6.75, and 9 °C warming at a temperate peatland ecosystem. Compared with previous studies on the SSP scenarios or similar climate projections [2,42], our projected CH_4 emissions under SSP1–2.6 and SSP2–4.5 have comparable increases but showed much stronger response under SSP5–8.5. It can be explained by

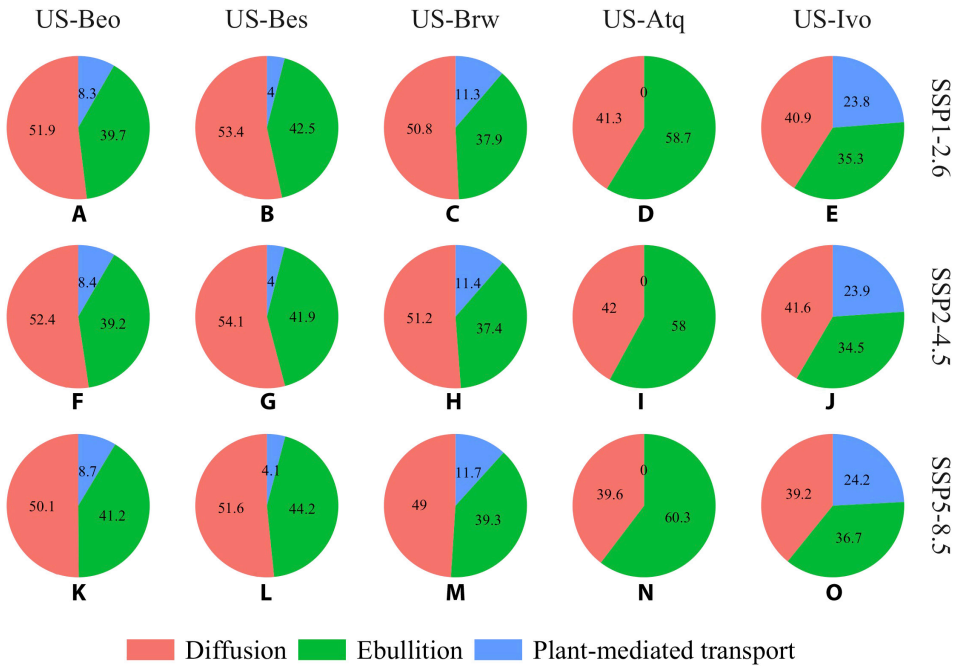

Fig. 3. Contribution of three transport pathways to total CH_4 fluxes during 2016–2025 at US-Beo, US-Bes, US-Brw, US-Atq, and US-Ivo under (A to E) SSP1–2.6, (F to J) SSP2–4.5, and (K to O) SSP5–8.5 scenarios.

changes in other climate factors that strengthened CH_4 emissions. Unchanged soil water levels or increased precipitation along with warming could cause greater increases in CH_4 emissions [13,40]. Shindell et al. [40] found that annual-average CH_4 emissions doubled with a fixed wetland distribution due to around 0.4 to 0.8 mm day^{-1} (annually 146 to 292 mm) precipitation increases with doubled CO_2 concentration over northern Eurasia. In this study, precipitation is annually increased by 41 to 48 mm $year^{-1}$ (24 to 30%), 58 to 66 mm $year^{-1}$ (33 to 45%), and 143 to 241 mm $year^{-1}$ (83 to 116%) under SSP1–2.6, SSP2–4.5, and SSP5–8.5, respectively (Fig. S6). Thus, simultaneous increases in temperature and precipitation yield a stronger promotion impact on CH_4 emissions than the warming-only scenario.

In this study, air temperature (67%) and precipitation (61%) act as the main factors to separately explain variations in CH_4 emissions (Table S7). Compared with Utqiaġvik sites, US-Ivo has smaller increases in temperature but larger increases in precipitation, and its CH_4 emissions exhibit a 17 to 38% greater increase (Fig. 2). Additionally, air temperature at US-Ivo is lower than at Utqiaġvik sites (Fig. S5). Thus, enhanced precipitation could result in this stronger CH_4 response; however, the strength of precipitation effects is hard to evaluate because of their interactions with warming and other climate factors on CH_4 emissions. Furthermore, more precipitation does not necessarily increase soil moisture, and the depth of waterlogged soils facilitated CH_4 production. Among all five sites, soil moisture is projected to increase under different SSP scenarios; however, the soil water table is deepened probably due to enhanced ET under warming (Fig. S1), which might cause a shrinkage of inundated (i.e., anaerobic) soil volume. Stronger ET is related to the reduction in CH_4 emissions, which can explain about 40% of variations in CH_4 emissions (Table S6). Our previous study finds that the soil water table level is reduced under warming due to hydrological feedback, therefore mitigating the stimulating effects of warming on CH_4 emissions [43]. Therefore, precipitation impacts are significantly more uncertain than warming impacts in predicting CH_4 emissions in Arctic regions.

Both CH_4 production and oxidation are microbiological processes affected by soil C input, soil temperature, and aerobic versus anaerobic conditions. Therefore, under different SSP scenarios, CH_4 emissions are also affected by vegetation and microbial activities [5,11]. Our results show that about 20% of variations in CH_4 emissions can be explained by NPP (Table S7). NPP can influence the amount of soil C inputs and SOM/DOC concentrations further to regulate CH_4 production and emission, but its strength is limited because the availability of soil C for methanogenesis depends on microbial decomposition rates [17]. CH_4 production is profoundly strengthened under SSP5–8.5 compared with SSP1–2.6 and SSP2–4.5. Additionally, increases in the rate of acetoclastic methanogenesis are more than 10 times greater than the rate of hydrogenotrophic methanogenesis under different SSP scenarios. Therefore, acetoclastic methanogenesis, the main pathway of CH_4 production, displays a stronger response to future climate change than hydrogenotrophic methanogenesis, likely due to higher acetate production under warmer conditions (Fig. 2). Moreover, increases in the rate of aerobic CH_4 oxidation are much smaller relative to CH_4 production, and its effects could be ignored in CH_4 emissions. Anaerobic oxidation is decelerated, which indicates that less CH_4 is consumed by methanotrophs and more preserved in soils. Furthermore, the CH_4 transport pathways are also accelerated under SSP scenarios, but their increases are less than in the input of soil CH_4 concentrations from enhanced production and reduced oxidation. As a result, soil CH_4 concentrations gradually grow by 2100 under different SSP scenarios with more concentrations under stronger warming scenarios. Of three CH_4 transport pathways, ebullition increases faster than plant-mediated transport and diffusion and finally dominates

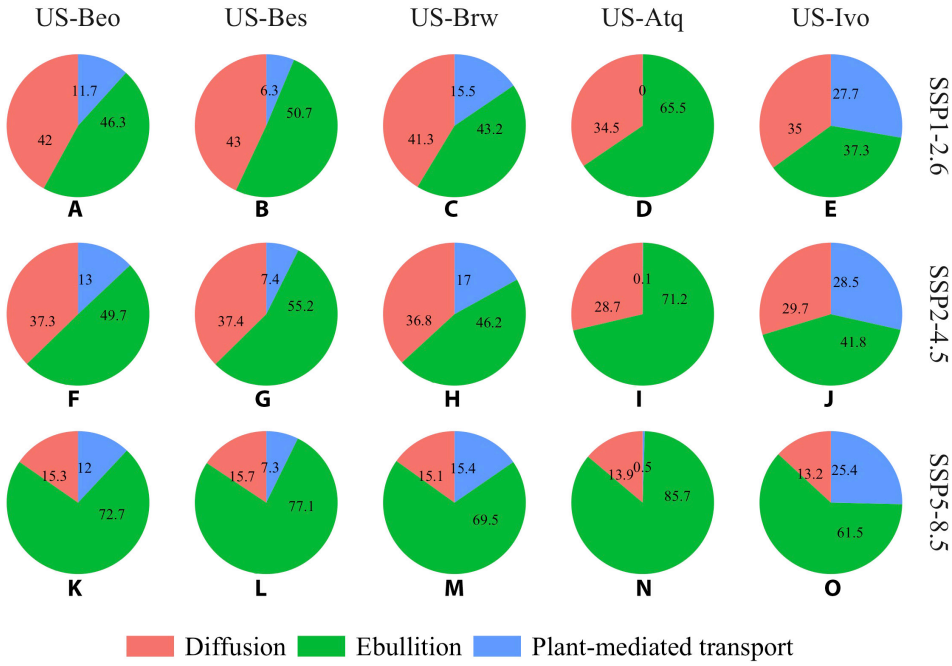

Fig. 4. Contribution of three transport pathways to total CH_4 fluxes in the 2090s at US-Beo, US-Bes, US-Brw, US-Atq, and US-Ivo under (A to E) SSP1–2.6, (F to J) SSP2–4.5, and (K to O) SSP5–8.5 scenarios.

the CH_4 transport under all considered SSP scenarios (Fig. 3). In the CLM-Microbe model, diffusion is determined by the differences in CH_4 concentrations between the atmosphere and soil pores, which are slightly affected by temperature and precipitation [29]. The plant-mediated transport and ebullition can be largely influenced by warming and enhanced precipitation. Plant-mediated transport is controlled by soil CH_4 concentrations, NPP, and root factions, whereas ebullition is affected by soil CH_4 concentrations and plant cover. Goodrich et al. [44] reported that higher ebullition rates in the summer were likely related to both higher rates of CH_4 production and the reduced solubility of CH_4 at higher temperatures. In our projection, changes in plant cover and composition cannot be simulated in the current version of the CLM-Microbe model; therefore, the substantial increase in ebullition is caused by the accumulation of soil CH_4 concentrations. In addition, the accelerated plant-mediated transport is partially caused by the increased NPP.

Differences in future CH_4 emissions across study sites

Projected CH_4 emissions gradually grow under three SSP scenarios across all five sites, and by 2100, the emissions are largest at US-Atq and lower at US-Beo and US-Bes (Table S4). The initial conditions of climate and environmental factors could affect the magnitude of increases in CH_4 emissions. Warmer and wetter conditions at US-Atq correspond with greater initial CH_4 emissions than other sites; moreover, projected CH_4 emissions at US-Atq show a stronger response to climate warming. It indicates that more attention should be paid to the areas with large CH_4 emissions because they can be affected by climate change to a greater extent. Plant cover also affect the responses of CH_4 emissions to climate change, despite that its effects are limited. For example, US-Atq has 73% of plant cover, the smallest among the five sites, leading to litter increases and ignorable contributions of plant-mediated transport to total CH_4 emissions over time (Figs. 2B, 3, and 4 and Fig. S9). Similarly, Utqiaġvik sites have more than 80% plant cover, corresponding to greater increases in plant-mediated transport and larger contributions to emissions among the five sites. Besides, although US-Ivo has lower plant cover (i.e., 78%) than Utqiaġvik sites, plant-mediated transport increases most and contributed most to CH_4 emissions among the five sites. The plant impacts primarily operate through root exudate, expressed as higher root fractions at US-Ivo than at other sites [27] (Fig. S2). Studies find that vegetation significantly enhanced CH_4 production via the substrate and stimulated CH_4 emission via plant-mediated transport [20,29].

Differences in future CH_4 emissions among climate models

Projected CH_4 emissions differ among five sites under the three SSP scenarios based on climate data derived from BCC-CSM2-MR, CESM2, and EC-Earth3. CH_4 emissions from Arctic regions tend to increase with temperature; therefore, the Q_{10} of CH_4 emissions is an essential parameter for estimating CH_4 emissions and CH_4–climate feedback under a warming climate. Our study reports distinct temperature sensitivities of CH_4 emissions under SSP1–2.6, SSP2–4.5, and SSP5–8.5 at one site based on one climate model. In most cases, CH_4 emissions is more sensitive to temperature under warmer scenarios based on BCC-CSM2-MR and CESM2 (Fig. 5), which is more consistent with Q_{10} for CH_4 production rather than precipitation and soil moisture (Figs. S11 to S14). It indicates that based on those two climate models, CH_4 production might be the main constraint for CH_4 emissions. However, CH_4 emissions are most sensitive to temperature under SSP1–2.6 than the other two warmer SSP scenarios based on EC-Earth3, which is most likely

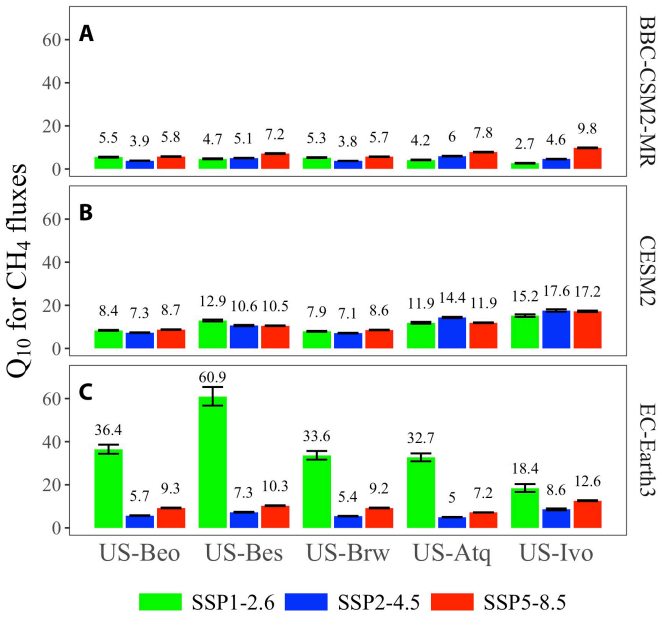

Fig. 5. Temperature sensitivity (Q_{10}) of CH_4 fluxes (mean ± SD; $n = 85$) at US-Beo, US-Bes, US-Brw, US-Atq, and US-Ivo under SSP scenarios derived from (A) BCC-CSM2-MR, (B) CESM2, and (C) EC-Earth3 models. Green indicates the SSP1–2.6 scenario, blue indicates the SSP2–4.5 scenario, and red indicates the SSP5–8.5 scenario. Numbers above the rectangular bar are values of Q_{10}; the error bar represents one unit of standard deviation.

affected by precipitation and soil moisture (Figs. S11 to S14). Because Q_{10} values for precipitation and soil moisture are significantly larger under SSP1–2.6 than SSP2–4.5 and SSP5–8.5, their effects are strong enough to promote Q_{10} for CH_4 production under SSP1–2.6. It indicates that changes in precipitation and soil moisture determine the contributions and constraints of CH_4 production on emission. Gill et al. [45] estimated the mean CH_4 flux Q_{10} to be 5.63 (2.92 to 10.52 with a 95% confidence interval) using a linearized Q_{10} function at the SPRUCE site during the 2015 growing season. Ma et al. [13] also reported a constrained Q_{10} range of 2.34 to 6.33 with a 95% confidence interval for CH_4 emissions. Q_{10} values for CH_4 emissions generally fell in the Q_{10} ranges for emissions but were higher than CH_4 production reported in previous studies. Our study reported a much stronger response of CH_4 emissions to warming, probably because we calculated the apparent Q_{10} rather than intrinsic Q_{10}, which can be enlarged by synchronous changes in precipitation under SSP scenarios [37]. Apparent Q_{10} values for CH_4 emission were lower using BCC-CSM2-MR (2.7 to 9.8) and higher using CESM2 (7.1 to 17.6) and EC-Earth3 (5 to 60.9) (Fig. 5). The selection of climate models may not affect the trends of projected CH_4 emissions, but it can impact temperature sensitivities for CH_4 emissions. In addition, to mitigate the uncertainties in CH_4 emissions under SSP scenarios, we should involve multiple climate models for future CH_4 projections.

Implications

This study demonstrates three major implications for CH_4 emission projections of SSP scenarios in Arctic ecosystems. First, the CLM-Microbe model projects Arctic CH_4 emissions from 2016 to 2100 at the landscape scale under SSP1–2.6, SSP2–4.5, and SSP5–8.5. CH_4 emissions are projected to significantly increase under SSP5–8.5 and are estimated to grow by a factor of 5.3 to 7.5 under SSP5–8.5 across the five Arctic sites. Second, this study demonstrates the mechanisms of future CH_4 dynamics with detailed information on CH_4 processes and environmental variables for the five study sites under different SSP scenarios. Our projected CH_4 emissions respond more strongly to rising temperatures than previous studies [13,40], highlighting the strong positive Arctic–CH_4 feedback, which is attributable to the precipitation-induced expansion of anoxic soils facilitating methanogenesis. Previous studies did not include microbial mechanisms, while our model explicitly represents methanogens that are sensitive to warming [18,20]. Ebullition is the main pathway for CH_4 transport across the five sites with climate impacts under SSP scenarios. Third, this study emphasizes the importance of including different climate datasets for CH_4 projections, which can help mitigate the uncertainties of CH_4 flux. Model simulations have different responses to the multiple climate datasets (BCC-CSM2-MR, CESM2, and EC-Earth3); even a slight difference in temperature or precipitation induces changes in CH_4 processes and their factors, leading to a significant change in CH_4 emissions. The key novelty of this study is that we developed a comprehensive understanding of microbial mechanisms of the intensified climate–CH_4 feedback in the Arctic tundra ecosystems under a warming climate.

Limitations and future work

Previous and current studies have validated the CLM-Microbe model in simulating contemporary and future CH_4 emissions at the landscape scale in the Arctic tundra by incorporating different upscaling techniques [6,14]. Here, we identify several limitations that need to be addressed in future research. First, vegetation shifts in shrub growth and abundance have been observed and modeled in the Arctic tundra [46]. The shrub expansion may affect tundra C balance by enhancing ecosystem C sequestration and altering ecosystem respiration through complex feedback mechanisms that affect snowpack dynamics, permafrost degradation, surface energy balance, and litter inputs [47]. However, our projection does not simulate the effects of shrub expansion, which could underestimate CH_4 emissions. Shrub expansion induces a deeper snowpack that may deepen the active layer [48], increasing soil wetness and soil anoxic conditions that enhance the CH_4 production [49]. Hence, the accuracy of CH_4 projections can be improved considering shifts in shrub cover under rapid Arctic warming. Second, permafrost underlies ~25% of the Northern Hemisphere land surface and stores an estimated ~1,700 Pg (1,700 Gt) of C in the frozen ground [50]. Permafrost thaws due to warming-induced expansion of anoxic conditions that increase CH_4 emissions [11,42]. Our projected CH_4 emissions might be underestimated without explicitly considering permafrost thaw, especially under strong warming scenarios. Thus, adding a module for permafrost thaw and permafrost C–climate feedback in the CLM-Microbe model could improve CH_4 projection under different SSP scenarios. Third, hydrological processes are critically important in determining the production, oxidation, and transport pathways of CH_4. Warming might lead to water table drawdown, suppressing CH_4 emission [43]. This feedback needs to be further investigated in the Alaskan Arctic tundra. Fourth, this study explored future CH_4 dynamics and the influence of various CH_4 processes on emissions that benefited from the CLM-Microbe model,

including different microbial functional groups (methanogens versus methanotrophs). In addition, incorporating various climate models can reduce the uncertainties of future CH_4 emissions. Based on the current study, integrated modeling efforts provide a reasonable approach to project CH_4 dynamics and budgets for the Arctic and globe for different climate trajectories and further ascertain the mechanisms of future CH_4 emissions.

Conclusion

This study applied the CLM-Microbe model to project future CH_4 emissions in five Arctic tundra sites under SSP1–2.6, SSP2–4.5, and SSP5–8.5 scenarios projected by three climate models. The study forecasts a significant increase in CH_4 emission in the Arctic ecosystem under warming climate, forming intensified CH_4–warming feedback. Model-projected CH_4 emissions increased by a factor of 5.3 to 7.5 under the SSP5–8.5 scenario while remaining relatively consistent with current emissions under SSP1–2.6 and SSP2–4.5 scenarios. Positive feedback to warming was noted for both acetoclastic methanogenesis and hydrogenotrophic methanogenesis: Warming climate led to higher CH_4 production. Microbial physiology and substrate availability dominated the positive feedback. Ebullition rates increased and acted as the dominant CH_4 transport pathway under all climate scenarios.

This study stands as a pioneering effort to decipher microbial mechanisms that reinforce the feedback loop between CH_4 and climate in the Arctic. By modeling methanogenesis and methanotroph activity, we aim to establish a thorough and mechanistic comprehension of CH_4 cycling in the Arctic, thereby providing a foundation for future microbial ecology studies in the context of climate change. The simulated amplification of positive feedback observed in the Arctic, driven by increased CH_4 emissions, highlights the urgency for policy interventions to curb this emission, a call to action made more pressing by the recent spike in CH_4 emissions.

Acknowledgments

We are grateful to R. A. Dahlgren from the University of California, Davis for his constructive suggestions in the early phase of this study.
Funding: We are grateful for the financial and facility support from San Diego State University. Financial assistance was partially provided by the SPRUCE and NGEE Arctic projects, which are supported by the Office of Biological and Environmental Research in the Department of Energy Office of Science. This project is partially supported by the U.S. National Science Foundation (2145130, 1702797, and 2208656). Geospatial support for this work was provided by the Polar Geospatial Center under NSF OPP awards 1204263 and 1702797. W.O. and D.Z. have been supported by NASA ABoVE program (NNX15AT74A and NNX16AF94A) and the National Oceanic and Atmospheric Administration NOAA/EPP Grant (NA22SEC4810016).
Author contributions: X.X. conceived the idea. Y.W. carried out all modeling experiments. L.H. and J.L. contributed to model forcing data. K.A., D.Z., D.L., and W.O. contributed observational data. J.L.R., D.M.R., and S.D.W. contributed to the interpretation of the results. Y.W. and X.X. led the writing of the early draft. All authors contributed to the manuscript revision.
Competing interests: The authors declare that they have no competing interests.

Data Availability

The code of the CLM-Microbe is archived on GitHub (https://github.com/email-clm/clm-microbe), which is publicly accessible to anyone who is interested. The data used in this study have been archived for US-Beo, US-Bes, US-Brw, US-Atq, and US-Ivo, which are available at https://daac.ornl.gov/ABOVE/guides/AK_North_Slope_NEE_CH4_Flux.html.

Supplementary Materials

Figs. S1 to S14
Tables S1 to S6

References

1. IPCC, Summary for policymakers. In: Masson-Delmotte V, Zhai P, Pirani A, Connors SL, Pean C, Chen Y, Goldfarb L, Gomis M, Matthews JBR, Berger S, et al., editors. *Climate change 2021: The physical science basis. Contribution of Working Group I to the Sixth Assessment Report of the Intergovernmental Panel on Climate Change*. Cambridge, United Kingdom and New York, NY, USA: Cambridge University Press; 2021.
2. Dean JF, Middelburg JJ, Röckmann T, Aerts R, Blauw LG, Egger M, Jetten MS, de Jong AE, Meisel OH, Rasigraf O, et al. Methane feedbacks to the global climate system in a warmer world. *Rev. Geophys*. 2018;56(1):207–250.
3. Lan X, Thoning K, Dlugokencky E. Trends in globally-averaged CH_4, N_2O, and SF6 determined from NOAA Global Monitoring Laboratory measurements. 2022. Version 2024-03, https://doi.org/10.15138/P8XG-AA10..
4. Nisbet EG, Manning M, Dlugokencky E, Fisher R, Lowry D, Michel S, Myhre CL, Platt SM, Allen G, Bousquet P, et al. Very strong atmospheric methane growth in the 4 years 2014–2017: Implications for the Paris agreement. *Global Biogeochem. Cycles*. 2019;33(3):318–342.
5. Oh Y, Zhuang Q, Liu L, Welp LR, Lau MC, Onstott TC, Medvigy D, Bruhwiler L, Dlugokencky EJ, Hugelius G, et al. Reduced net methane emissions due to microbial methane oxidation in a warmer Arctic. *Nat Clim Chang*. 2020;10:317–321.
6. Wang Y, Yuan F, Arndt KA, Liu J, He L, Zuo Y, Zona D, Lipson DL, Oechel WC, Ricciuto DM, et al. Upscaling methane flux from plot-level to eddy covariance tower domains in five Alaskan Tundra ecosystems. *Front. Environ. Sci*. 2022;10: Article 939238.
7. Kirschke S, Bousquet P, Ciais P, Saunois M, Canadell JG, Dlugokencky EJ, Bergamaschi P, Bergmann D, Blake DR, Bruhwiler L, et al. Three decades of global methane sources and sinks. *Nat. Geosci*. 2013;6(10):813–823.
8. Koven CD, Ringeval B, Friedlingstein P, Ciais P, Cadule P, Khvorostyanov D, Krinner G, Tarnocai C. Permafrost carbon-climate feedbacks accelerate global warming. *Proc. Natl. Acad. Sci. U.S.A*. 2011;108(36):14769–14774.
9. Lawrence D, Koven C, Swenson S, Riley W, Slater A. Permafrost thaw and resulting soil moisture changes regulate projected high-latitude CO_2 and CH_4 emissions. *Environ. Res. Lett*. 2015;10(9):Article 094011.
10. Hansen J, Sato M, Kharecha P, Russell G, Lea DW, Siddall M. Climate change and trace gases. *Philos Trans A Math Phys Eng Sci*. 1856;2007(365):1925–1954.
11. Miner KR, Turetsky MR, Malina E, Bartsch A, Tamminen J, McGuire AD, Fix A, Sweeney C, Elder CD, Miller CE.

Permafrost carbon emissions in a changing Arctic. *Nat Rev Earth Environ*. 2022;3(1):55–67.
12. Turetsky MR, Treat CC, Waldrop MP, Waddington JM, Harden JW, McGuire AD. Short-term response of methane fluxes and methanogen activity to water table and soil warming manipulations in an Alaskan peatland. *J. Geophys. Res*. 2008;113(G3).
13. Ma S, Jiang J, Huang Y, Shi Z, Wilson RM, Ricciuto D, Sebestyen SD, Hanson PJ, Luo Y. Data-constrained projections of methane fluxes in a northern Minnesota peatland in response to elevated CO_2 and warming. *J. Geophys. Res. Biogeo*. 2017;122(11):2841–2861.
14. Wang Y, Yuan F, Yuan F, Gu B, Hahn MS, Torn MS, Ricciuto DM, Kumar J, He L, Zona D, et al. Mechanistic modeling of microtopographic impacts on CO_2 and CH_4 fluxes in an Alaskan tundra ecosystem using the CLM-microbe model. *J Adv Model Earth Syst*. 2019;11:4228–4304.
15. Arndt KA, Oechel WC, Goodrich JP, Bailey BA, Kalhori A, Hashemi J, Sweeney C, Zona D. Sensitivity of methane emissions to later soil freezing in Arctic tundra ecosystems. *J. Geophys. Res. Biogeo*. 2019;124(8):2595–2609.
16. Bao T, Jia G, Xu X. Wetland heterogeneity determines methane emissions: A pan-arctic synthesis. *Environ. Sci. Technol*. 2021;55(14):10152–10163.
17. Xu X, Yuan F, Hanson PJ, Wullschleger SD, Thornton PE, Riley WJ, Song X, Graham DE, Song C, Tian H. Review and synthesis: Four decades of modeling methane cycling within terrestrial ecosystems. *Biogeosciences*. 2016;13(12):3735–3755.
18. Xu X, Elias DA, Graham DE, Phelps TJ, Carrol SL, Wullschleger SD, Thornton PE. A microbial functional group based module for simulating methane production and consumption: Application to an incubation permafrost soil. *Eur. J. Vasc. Endovasc. Surg*. 2015;120(6):1315–1333.
19. He L, Lipson DL, Rodrigues JL, Mayes MA, Bjork RG, Glaser B, Thornton P, Xu X. Dynamics of fungal and bacterial biomass carbon in natural ecosystems: Site-level applications of the CLM-microbe model. *J Adv Model Earth Syst*. 2021;13:e2020MS002283.
20. He L, Lai C-T, Mayes MA, Murayama S, Xu X. Microbial seasonality promotes soil respiratory carbon emission in natural ecosystems: A modeling study. *Glob. Chang. Biol*. 2021;27(13):3035–3051.
21. Xu X, Schimel JP, Thornton PE, Song X, Yuan F, Goswami S. Substrate and environmental controls on microbial assimilation of soil organic carbon: A framework for earth system models. *Ecol. Lett*. 2014;17(5):547–555.
22. Koven CD, Riley W, Subin ZM, Tang J, Torn MS, Collins WD, Bonan GB, Lawrence DM, Swenson SC. The effect of vertically-resolved soil biogeochemistry and alternate soil C and N models on C dynamics of CLM4. *Biogeosci Discuss*. 2013;10(11):7201–7256.
23. Thornton PE, Rosenbloom NA. Ecosystem model spin-up: Estimating steady state conditions in a coupled terrestrial carbon and nitrogen cycle model. *Ecol. Model*. 2005;189(1–2):25–48.
24. Davidson SJ, Santos MJ, Sloan VL, Reuss-Schmidt K, Phoenix GK, Oechel WC, Zona D. Upscaling CH_4 fluxes using high-resolution imagery in Arctic tundra ecosystems. *Remote Sens. (Basel)*. 2017;9(12):1227.
25. Arndt KA, Lipson DA, Hashemi J, Oechel WC, Zona D. Snow melt stimulates ecosystem respiration in Arctic ecosystems. *Glob. Chang. Biol*. 2020;26(9):5042–5051.
26. Zona D, Gioli B, Commane R, Lindaas J, Wofsy SC, Miller CE, Dinardo SJ, Dengei S, Sweeney C, Karion A, et al. Cold season emissions dominate the Arctic tundra methane budget. *Proc. Natl. Acad. Sci. USA*. 2016;113(1):40–45.
27. Davidson SJ, Sloan VL, Phoenix GK, Wagner R, Fisher JP, Oechel WC, Zona D. Vegetation type dominates the spatial variability in CH_4 emissions across multiple Arctic tundra landscapes. *Ecosystems*. 2016;19(6):1116–1132.
28. Walker D, Binnian E, Evans B, Lederer N, Nordstrand E, Webber P. Terrain, vegetation and landscape evolution of the R4D research site, Brooks Range foothills Alaska. *Holarctic Ecol*. 1989;12(3):238–261.
29. Xu X, He L, Wang Y, CLM-microbe v1.0. Zenodo. 2022. https://doi.org/10.5281/zenodo.7439312.
30. Meinshausen M, Nicholls ZR, Lewis J, Gidden MJ, Vogel E, Freund M, Beyerle U, Gessner C, Nauels A, Bauer N, et al. The shared socio-economic pathway (SSP) greenhouse gas concentrations and their extensions to 2500. *Geosci. Model Dev*. 2020;13(8):3571–3605.
31. Nazarenko L, Schmidt G, Miller R, Tausnev N, Kelley M, Ruedy R, Russell G, Aleinov I, Bauer M, Bauer S, et al. Future climate change under RCP emission scenarios with GISS M odelE2. *J Adv Model Earth Syst*. 2015;7(1): 244–267.
32. Langford ZL, Kumar J, Hoffman FM, Breen AL, Iversen CM. Arctic vegetation mapping using unsupervised training datasets and convolutional neural networks. *Remote Sens. (Basel)*. 2019;11(1):69.
33. Wilson C, Gangodagamage C, Rowland J. Digital elevation model, 0.5 m, Barrow Environmental Observatory, Utqiagvik (Barrow), Alaska 2012. Next Generation Ecosystems Experiment—Arctic, Oak Ridge National Laboratory; 2013.
34. Porter C, Morin P, Howat I, Noh M-J, Bates B, Peterman K, Keesey S, Schlenk M, Gardiner J, Tomko K, et al. ArcticDEM, Version 3, H. Dataverse, Editor. 2018.
35. Hugelius G, Bockheim J, Camill P, Elberling B, Grosse G, Harden J, Johnson K, Jorgenson T, Koven C, Kuhry P, et al. A new data set for estimating organic carbon storage to 3 m depth in soils of the northern circumpolar permafrost region. *Earth Syst Sci Data*. 2013;5(2):393–402.
36. Oleson K, Lawrence, DM, Bonan, GB, Drewniak, B, Huang, M, Koven, CD, Levis, S, Li, F, Riley, WJ, Subin, ZM, et al. Technical description of version 4.5 of the community land model (CLM). 2013.
37. Davidson EA, Janssens IA. Temperature sensitivity of soil carbon decomposition and feedbacks to climate change. *Nature*. 2006;440(7081):165–173.
38. Koffi EN, Bergamaschi P, Alkama R, Cescatti A. An observation-constrained assessment of the climate sensitivity and future trajectories of wetland methane emissions. *Sci. Adv*. 2020;6(15):eaay4444.
39. R Core Team, *R: A language and environment for statistical computing*. Vienna, Austria: R Foundation for Statistical Computing; 2020. https://www.r-project.org/.
40. Shindell DT, Walter BP, Faluvegi G. Impacts of climate change on methane emissions from wetlands. *Geophys. Res. Lett*. 2004;31(21):L21202.
41. Frolking S, Crill P. Climate controls on temporal variability of methane flux from a poor fen in southeastern New Hampshire: Measurement and modeling. *Global Biogeochem. Cycles*. 1994;8(4):385–397.
42. Anisimov OA. Potential feedback of thawing permafrost to the global climate system through methane emission. *Environ. Res. Lett*. 2007;2:Article 045016.

43. Yuan F, Wang Y, Ricciuto DM, Shi X, Yuan F, Brehme T, Bridgham S, Keller JK, Warren JM, Griffiths NA, et al. Hydrological feedbacks on peatland CH_4 emission under warming and elevated CO_2: A modeling study. *J. Hydrol*. 2021;603:127137.
44. Goodrich JP, Varner RK, Frolking S, Duncan BN, Crill PM. High-frequency measurements of methane ebullition over a growing season at a temperate peatland site. *Geophys. Res. Lett*. 2011;38(7).
45. Gill AL, Giasson MA, Yu R, Finzi AC. Deep peat warming increases surface methane and carbon dioxide emissions in a black spruce dominated ombrotrophic bog. *Glob. Chang. Biol*. 2017;23(12):5398–5411.
46. Tremblay B, Lévesque E, Boudreau S. Recent expansion of erect shrubs in the low Arctic: Evidence from eastern Nunavik. *Environ. Res. Lett*. 2012;7(3):Article 035501.
47. Mekonnen ZA, Riley WJ, Berner LT, Bouskill NJ, Torn MS, Iwahana G, Breen AL, Myers-Smith IH, Criado MG, Liu Y, et al. Arctic tundra shrubification: A review of mechanisms and impacts on ecosystem carbon balance. *Environ. Res. Lett*. 2021;16(5):Article 053001.
48. Nitzbon J, Westermann S, Langer M, Martin LC, Strauss J, Laboor S, Boike J. Fast response of cold ice-rich permafrost in Northeast Siberia to a warming climate. *Nat. Commun*. 2020;11(1):2201.
49. Blanc-Betes E, Welker JM, Sturchio NC, Chanton JP, Gonzalez-Meler MA. Winter precipitation and snow accumulation drive the methane sink or source strength of Arctic tussock tundra. *Glob. Chang. Biol*. 2016;22(8):2818–2833.
50. Olefeldt D, Goswami S, Grosse G, Hayes D, Hugelius G, Kuhry P, McGuire AD, Romanovsky V, Sannel ABK, Schuur E, et al. Circumpolar distribution and carbon storage of thermokarst landscapes. *Nat. Commun*. 2016;7(1):13043.